https://doi.org/10.5194/wes-2022-82
Preprint. Discussion started: 20 September 2022

eawe european academy of wind energy
Open Access WIND ENERGY SCIENCE DISCUSSIONS

A Neighborhood Search Integer Programming Approach for Wind Farm Layout Optimization

Juan-Andrés Pérez-Rúa[1], Mathias Stolpe[1], and Nicolaos Antonio Cutululis[1]

[1] Department of Wind and Energy Systems, Technical University of Denmark, Frederiksborgvej 399, 4000 Roskilde, Denmark

Correspondence: Juan-Andrés Pérez-Rúa (juru@dtu.dk)

Abstract. Two models and a heuristic algorithm to address the wind farm layout optimization problem are presented. The models are linear integer programming formulations where candidate locations of wind turbines are described by binary variables. One formulation considers an approximation of the power curve by means of a step-wise constant function. The other model is based on a power-curve-free model where minimization of a measure closely related to total wind speed deficit is aimed. A special-purpose neighborhood search heuristic wraps the formulations in order to increase tractability and effectiveness compared to the full model. The heuristic iteratively searches neighborhoods around the incumbent using a branch-and-cut algorithm. The number of candidate locations and neighborhood sizes are adjusted adaptively. Numerical results on a set of publicly available benchmark problems indicate that a proxy for total velocity deficit as objective is a functional approach, since high-quality solutions of an annual energy production metric are found. Furthermore, the proposed heuristic is able to match and in some cases improve the results obtained when considering the turbine positions as continuous variables.

1 Introduction

Cost reductions for renewable energy generation is on the top of political agendas, with the objective of supporting the worldwide proliferation of clean energy production systems. Subsidy-free tendering processes become more frequent, as is the case for offshore wind auctions in Germany since 2017 and in Netherlands since 2018, or in China for onshore wind from 2021 (GWEC, 2020a). The fast evolution of offshore wind in the last decade, with an sharp growth of global installed capacity (GWEC, 2020b), is yet another clear indicator of the maturity of the industry. As wind energy is unleashing its potential to contribute for a successful green energy transition, the need to further economically refine wind farm designs turns into a crucial task.

The basic Wind Farm Layout Optimization (WFLO) problem consists in deciding the positioning of Wind Turbines (WTs) within a given project area to maximize the Annual Energy Production (AEP) while respecting a minimum separation distance between the generators. The classic problem definition is to place a fixed number n_{T} of homogeneous (single type) WTs. This problem has been studied broadly and intensively since at least three decades (Herbert-Acero et al., 2014). The first effort in the topic was the pioneering work of Mosetti et al. (Mosetti et al., 1994), where the Katic-Jensen wake decay model (Katic

https://doi.org/10.5194/wes-2022-82
Preprint. Discussion started: 20 September 2022

eawe european academy of wind energy
Open Access WIND ENERGY SCIENCE DISCUSSIONS

et al., 1986), implemented to compute wake losses, is coupled with a genetic algorithm (Deb, 2013) as optimizer to iteratively improve the layout.

In this perspective, the main components when building an optimization workflow for the WFLO problem are the wake and the optimization models, and the associated numerical algorithms. For the first, in order to be able to formulate tractable frameworks, the designer needs to rely on the so-called engineering models. These are essentially mathematical representations which can be expressed in terms of analytical equations after greatly simplifying complex physics modelling, while still capturing at a good extent the underlying nature of the phenomenon under analysis. Recently, scientific articles in this field have proposed and validated engineering wake models with smooth and differentiable velocity deficit shape, as the Bastankhah's Gaussian (Bastankhah and Porté-Agel, 2016) or its simplified version (Thomas and Ning, 2018), the Niayifar and Porté-Agel (Niayifar and Porté-Agel, 2015) or the Jensen cosine model (Thomas et al., 2022b). Likewise, the aggregation of individual wake velocity deficits can be done through linear superposition or root sum squares (Porté-Agel et al., 2020).

Optimization techniques for the WFLO problem can be classified, depending on the choice of variables, into continuous and discrete optimization. In the field of continuous optimization, the location $\mathbf{p}_i$ of a WT i, in terms of the abscissa (x_i) and ordinate variables (y_i) in the Cartesian plane, $\mathbf{p}_i = (x_i, y_i)$, can take any real values, while ensuring that the point is within the project area $\mathbf{F}$, and simultaneously satisfying the minimum distance constraints. Several gradient-free algorithms have been applied to this problem, including metaheuristics, as genetic algorithm (Réthoré et al., 2014) or particle swarm optimization (Wan et al., 2010). Likewise, gradient-based methods can be utilized for this problem, as for example the Sparse Nonlinear OPTimizer (SNOPT), that uses a Sequential Quadratic Programming (SQP) approach (Thomas et al., 2022a), or interior-point solvers (Pérez et al., 2013). In general, gradient-free algorithms, although highly flexible for modelling aspects, have considerably poorer scalability for larger problem sizes than gradient-based approaches. Re-parametrization approaches aiming to reduce the number of variables through simplified geometrical representations of the problem, such as row and column spacing or inclination angle, are also emerging within this context bringing along various enhancements (Stanley and Ning, 2019). Additionally, multi-start strategies are frequently implemented as a workaround for the intrinsic multi-modal nature of the WFLO problem. Finally, hybrid methods combining gradient-free and gradient-based algorithms are also an alternative able to come up with competitive results (Mittal and Mitra, 2017).

Discrete optimization models can be formulated for this problem by means of sampling the available project area in form of N candidate location points. Thus, only a set of finite options from the continuous search space are considered, where the n_T WTs are installable, with in principle $N \gg n_\mathrm{T}$. In contrast to continuous optimization, a candidate point i is then represented by a binary variable ξ_i, that gets a value of one if a WT is installed at that location, or zero otherwise. The vast majority of articles in the literature implement gradient-free algorithms for this technique, as the works of Mosetti et al. (Mosetti et al., 1994) and Grady et al. (Grady et al., 2005), where both use genetic algorithms. This modelling technique, however, fits very well in the well-studied general framework of integer programming. The main advantage of this approach is the possibility to utilize exact solvers based on branch-and-cut method; theoretically, being able to solve a problem to optimality while supporting common engineering constraints (Wolsey, 2020). Nevertheless, the low tractability and poor scalability of this method in function of the size of N and the number of state variables is well-known.

https://doi.org/10.5194/wes-2022-82
Preprint. Discussion started: 20 September 2022

eawe european academy of wind energy
Open Access WIND ENERGY SCIENCE DISCUSSIONS

Probably the first work within the context of integer programming for the WFLO problem was the thesis of Fagerfjäll in 2010 (Fagerfjäll, 2010), where a Mixed Integer Linear Program (MILP) is proposed, modelling the objective AEP function as a superposition of deficits defined in terms of power. Although physically inaccurate, as the deficit superposition should be computed for velocities, an important reduction in the number of variables is achieved that ultimately allow solving to optimality rather small problem instances. A similar approximation is carried out by Archer et al. (Archer et al., 2011), Fischetti et al. (Fischetti et al., 2016), and Quan et al. (Quan and Kim, 2019), but introducing important modifications to the model by reducing number of constraints. The objective function may also be formulated for aggregated velocity deficit (Turner et al., 2014; Kuo et al., 2016), but the imperfect correspondence with AEP will result in not solving the original problem to optimality, and possibly getting final low-quality solutions. Another advantage of integer programming formulations is the chance of incorporating heuristic routines in the top of such models, as for instance proximity search (Fischetti et al., 2016; Shaw, 1998), to quickly improve a given starting feasible point.

A large number of benefits are implicit in the discrete modelling technique over the continuous counterpart, including: (i) capacity to include the number of WTs as a variable and to model overall economic metrics as Net Present Value (NPV), (ii) capacity to easily model any shape of project area or forbidden zones, convex or non-convex, (iii) capacity to model extensive integrated models to support electrical systems optimization, (iv) capacity to easily model terrain-based constraints or cost functions, (v) capacity to incorporate multiple WT types, among others. These functionalities are the main motivation for this manuscript to focus on proposing new methods for the WFLO problem in the area of discrete optimization. Moreover, in broader terms, since even the basic definition of the WFLO problem translates into a non-convex formulation, in general new methods are required to efficiently come up with high-quality solutions.

Several contributions to the field of discrete optimization for WFLO are proposed in the manuscript. The first contribution is the proposition of new integer linear formulations which are able to capture to a good extent the underlying physics of the problem. The main obstacles for a MILP representation of WFLO problem are the non-linearity of the power curves, and the choice of wake velocity deficit superposition approach. Currently, the scientific literature in this context has fundamental knowledge gaps in at least one of these aspects. For example, previous works have considered aggregation of power deficits instead of velocities, gaining a simplification on the mathematical formulation, in detriment of the physics modelling fidelity. This article presents new strategies for modelling both facets in the class of MILP problems, one with explicit power curve and wake superposition modelling, and another with a proxy objective function based on total wind speed, thus simplifying the original formulation. The second main contribution is the proposition of a new special purpose neighborhood search heuristics in order to speed up the generation of high-quality solutions. This heuristic wraps both formulations having a twofold functionality, first to increase tractability, and second to redirect the optimization search in terms of a specified high-fidelity objective function. The main contributions of this research are both methodological and empirical. The main numerical results indicate good computational performances for a set of publicly available benchmark case studies compared to state-of-the-art gradient-free and gradient-based approaches (Baker et al., 2019).

Section 2 introduces the engineering models of the physical aspects of interest in the article. Section 3 presents the two mathematical programs developed, and Sect. 4 unfolds the proposed heuristic framework wrapping both programs. Computa-

https://doi.org/10.5194/wes-2022-82
Preprint. Discussion started: 20 September 2022

eawe european academy of wind energy
Open Access WIND ENERGY SCIENCE DISCUSSIONS

tional experiments are deployed in Sect. 5, followed up by discussions in Sect. 6, and lastly the manuscript is finalized with the conclusions in Sect. 7.

2 Physics Modelling

The proposed MILP models and general optimization framework in this article can be easily applied to many wake deficit models. No particular properties on smoothness or differentiability, or specific demands on mathematical structure are required in connection with controlling wake diameter and deficit (Thomas et al., 2022b). Since the computational results in the article are obtained after solving open access case studies from the IEA37 Wind Task 37 (Baker et al., 2019; Dykes et al., 2015), the implemented wake model from that source is presented in Sect. 2.1, along with the used superposition techniques in Sect. 2.2, WT power curve in Sect. 2.3, and the AEP calculation procedure in Sect. 2.4. Variations on ways of computing the absolute velocity deficits and linear wakes superposition under the framework of MILP are introduced as well.

2.1 Wake Model

A simplified version of the Bastankhah's Gaussian is considered (Thomas and Ning, 2018). The relative velocity deficit $\delta u_{i\ell} = \Delta u_{i\ell}/u_\infty = (u_\infty - u(\bar{x}_i, \bar{y}_i))/u_\infty$ behind a single WT located at ℓ, and evaluated at point i, is described using the model and notation from (IEA Wind Task 37, 2019).

$$\delta u_{i\ell} = \begin{cases} \left(1 - \sqrt{1 - \frac{C_\mathrm{T}}{8\sigma_\mathrm{y}^2/D^2}}\right) \exp\left(-0.5\left(\frac{\bar{y}_i - \bar{y}_\ell}{\sigma_\mathrm{y}}\right)^2\right), & \bar{x}_i - \bar{x}_\ell > 0 \\ 0, & \text{otherwise.} \end{cases} \tag{1}$$

$$\sigma_\mathrm{y} = k_\mathrm{y}(\bar{x}_i - \bar{x}_\ell) + D/\sqrt{8} \tag{2}$$

where u_∞ is the inflow wind speed, C_T is the thrust coefficient, $d_{ij}^{\parallel} = \bar{x}_i - \bar{x}_\ell$ is the stream-wise distance from the hub generating wake ($\bar{x}_\ell$) to hub of interest ($\bar{x}_i$) along freestream, $d_{ij}^{\perp} = \bar{y}_i - \bar{y}_\ell$ is the span-wise distance from the hub generating wake to hub of interest perpendicular to freestream, σ_y is the standard deviation of the wake deficit, k_y is a variable based on a turbulence intensity, and D is the WT diameter.

2.2 Wake velocity deficit superposition

The absolute velocity deficit $\Delta u_{i\ell}(\theta^j, k)$ at wind direction θ^j and wind speed k, $\Delta u_{i\ell}(\theta^j, k)$, can be estimated in two ways. Either it is based on the inflow wind speed through

$$\Delta u_{i\ell}(\theta^j, k) = \delta u_{i\ell}(\theta^j, k) u_\infty^k \tag{3}$$

or it is based on the wind speed $u_{\ell jk}$ at WT ℓ creating the wake at point i for wind direction θ^j and speed k,

$$\Delta u_{i\ell}(\theta^j, k) = \delta u_{i\ell}(\theta^j, k) u_{\ell jk} \tag{4}$$

https://doi.org/10.5194/wes-2022-82
Preprint. Discussion started: 20 September 2022

eawe european academy of wind energy
Open Access WIND ENERGY SCIENCE DISCUSSIONS

here $\delta u_{i\ell}(\theta^j, k)$ is the relative velocity deficit of i over j at same operation condition after Eq.(1) and Eq.(2). Note that Eq. (3) leads to a greater value and therefore is considered a conservative approach compared to (the potentially more realistic) Eq. (4) (Niayifar and Porté-Agel, 2015). Nonetheless, implementing Eq. (3) greatly simplifies the resultant system of equations and allow for preprocessing calculations.

Let the set $\boldsymbol{U}_i^{\theta^j}$ collects the WTs creating wake over WT at point i for wind direction θ^j and speed k as per

$$\boldsymbol{U}_i^{\theta^j} = \{\ell \,|\, \text{position } \ell \text{ is up-wind compared to position } i \text{ for wind direction } j\} \tag{5}$$

The wake velocity deficit superposition, to calculate the total velocity deficit at WT i, $\Delta u_i(\theta^j, k)$, can be obtained through two mechanisms. Either it is based on linear superposition model through

$$\Delta u_i(\theta^j, k) = \sum_{\ell \in \boldsymbol{U}_i^{\theta^j}} \Delta u_{i\ell}(\theta^j, k) \tag{6}$$

or it is based on the root sum squares superposition model

$$\Delta u_i(\theta^j, k) = \sqrt{\sum_{\ell \in \boldsymbol{U}_i^{\theta^j}} \Delta^2 u_{i\ell}(\theta^j, k)} \tag{7}$$

2.3 WT Power Curve

For computing AEP suitable power curves are required for the available turbine types. These power curves are often not perfectly suitable for optimization, due to the non-differentiability at rated wind speed. The general characteristics are that the power curve is zero below cut-in wind speed, zero above the cut-out wind speed, constant between the rated wind speed and the cut-out wind speed. In between the cut-in and rated wind speeds the curve is assumed to be smooth, convex and monotonically increasing. The simplified power curve for a generic turbine as a function of wind speed u is modelled through

$$p(u) = \begin{cases} 0, & u \le u^{\text{cut-in}} \\ p^{\text{rated}} \left(\frac{u - u^{\text{cut-in}}}{u^{\text{rated}} - u^{\text{cut-in}}} \right)^3, & u^{\text{cut-in}} \le u \le u^{\text{rated}} \\ p^{\text{rated}}, & u^{\text{rated}} \le u \le u^{\text{cut-out}} \\ 0, & u > u^{\text{cut-out}}. \end{cases} \tag{8}$$

where p^{rated} is the nominal power at (and above) rated wind speed u^{rated}. The other turbine characteristics are the cut-in wind speed $u^{\text{cut-in}}$, and the cut-out wind speed $u^{\text{cut-out}}$.

2.4 Annual Energy Production, AEP

The AEP is obtained after the application of the following expression

https://doi.org/10.5194/wes-2022-82
Preprint. Discussion started: 20 September 2022

eawe european academy of wind energy
Open Access WIND ENERGY SCIENCE DISCUSSIONS

$$AEP = 8760 \sum_{i=1}^{n_T} \sum_{j,k} w_{jk} p(u_{ijk}) \tag{9}$$

where w_{jk} is the joint probability of wind direction j and wind speed k, and 8760 is the number of hours of a standard year.

3 Optimization Models

The MILP model with explicit modelling of the WT power curve, wake model and wakes superposition is first introduced in Sect. 3.1. Then, the power-curve-free formulation, based on total wind speed within the farm, is deployed in Sect. 3.2.

For both models, the main type of variables $\xi_i \in \{0,1\}$ represent presence or absence of turbines at the candidate locations as mentioned before. Given N points, i.e. candidate locations for turbine positions, with positions $\mathbf{p}_i$ inside the domain $\mathbf{F}$ (i.e. $\mathbf{p}_i \in \mathbf{F}$ for all i WT candidate locations), binary variables $\xi_i \in \{0,1\}$ are associated with the following interpretation

$$\xi_i = \begin{cases} 1, & \text{if a turbine is located at point } i \text{ with position } \mathbf{p}_i, \text{ and} \\ 0, & \text{otherwise.} \end{cases} \tag{10}$$

Let the index sets $\boldsymbol{N}_i$ storing the candidate locations violating the minimum distance constraints for a WT i be defined as

$$\boldsymbol{N}_i = \{j \in \{1,\dots,n\}, j \neq i \mid d_{ij}(\mathbf{p}_i, \mathbf{p}_j) < d^{\min}\} \tag{11}$$

where $d^{\min} > 0$ is the minimum required distance between two turbines ($2D$ in this study). If $\xi_i = 1$ then all binary variables in the set $\boldsymbol{N}_i$ should be forced to zero, whereas if $\xi_i = 0$ these variables should be free to take any value in {0,1}.

All relevant distances can be preprocessed for all combinations of points i and j. These pertinent parameters are then defined as function of the Cartesian plane positions $\mathbf{p}$ and wind direction θ^j, as the Euclidean distances $d_{ij}(\mathbf{p}) = \|\mathbf{p}_i - \mathbf{p}_j\|_2$, the stream-wise distances $d_{ij}^{\parallel}(\mathbf{p};\theta^j)$ and the span-wise distances $d_{ij}^{\perp}(\mathbf{p};\theta^j)$, extending the concept introduced in Sect. 2.1.

3.1 Power-curve-based model

For the purpose of wake modelling and power computation continuous state variables u_{ijk} are used. A variable u_{ijk} represents the wind speed at WT location i, for wind direction j, and wind speed k.

The general characteristics of the power curve outlined in Sect. 2.3 is used to approximate the curve by a step-wise function. The cubic domain of the power curve is first partitioned into m intervals, plus one interval from a negative point ($-u^{\text{ini}}$) to the cut-in speed, and a final one to cover the range from rated to cut-out speed. Each isometric interval of length Δu is approximated with a constant power value, see Fig. 1.

An interval l is characterized by three parameters u_{s}^l, u_{m}^l, and u_{h}^l with the next properties

https://doi.org/10.5194/wes-2022-82
Preprint. Discussion started: 20 September 2022

eawe european academy of wind energy
Open Access WIND ENERGY SCIENCE DISCUSSIONS

$$u_{\mathrm{s}}^{1} = -u^{\text{ini}}, u_{\mathrm{h}}^{1} = u^{\text{cut-in}}, u_{\mathrm{s}}^{m+2} = u^{\text{rated}}, u_{\mathrm{h}}^{m+2} = u^{\text{cut-out}} \tag{12}$$

$$u_{\mathrm{s}}^{2} = u^{\text{cut-in}}, u_{\mathrm{h}}^{m+1} = u^{\text{rated}}, u_{\mathrm{s}}^{a+1} = u^{\text{cut-in}} + (a-1)\Delta u, u_{\mathrm{h}}^{a+1} = u^{\text{cut-in}} + a\Delta u \text{ for } a = 1, \ldots, m \tag{13}$$

$$u_{\mathrm{m}}^{l} = 0.5(u_{\mathrm{s}}^{l} + u_{\mathrm{h}}^{l}) \tag{14}$$

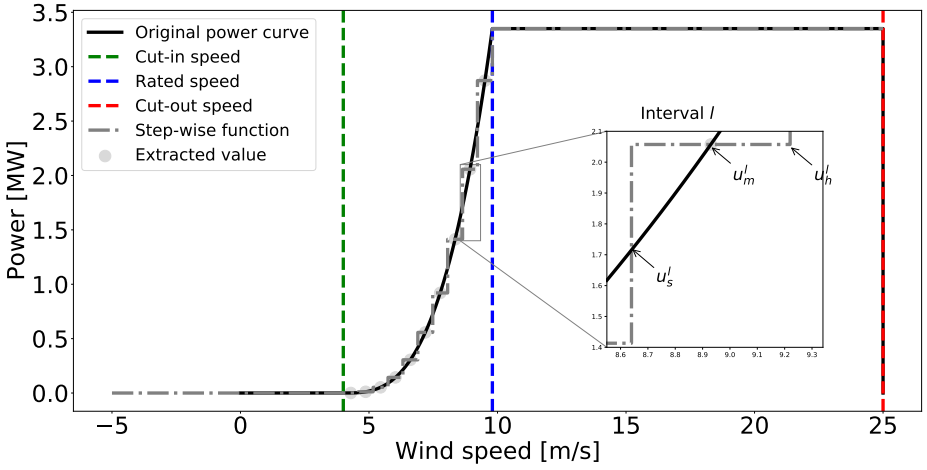

Figure 1. Piece-wise constant approximation of a wind turbine power curve through sampling with $m = 10$ intervals between the cut-in and rated wind speeds.

Equation (12) defines the lower and upper limits for the extreme intervals $l = 1$ and $l = m + 2$, Eq. (13) formalizes them for a interval l in the cubic part of the curve ($2 \leq l \leq m + 1$), and Eq. (14) presents how to determine the extracted wind speed associated to the power value in l, which is the average value of u_{s}^{l} and u_{h}^{l}.

Let define the binary state variables $\eta_{ijk}^{l} \in \{0, 1\}$ for $l = 1, \ldots, m + 2$ with the interpretation

$$\eta_{ijk}^{l} = \begin{cases} 1, & \text{if } u_{\mathrm{s}}^{l} \leq u_{ijk} \leq u_{\mathrm{h}}^{l}, \text{ and} \\ 0, & \text{otherwise.} \end{cases} \tag{15}$$

i.e. these variables indicate which of the wind speed intervals l of the power curve approximation for WT i, operates at wind direction j, and wind speed k.

After the presentation of all the variables of the model, activation variables ξ, continuous state variables u, and binary state variables η, the formulation in Eq. (16) collects the AEP objective function, the constraints of a generalized version of the WFLO problem, and the variables' domain definition.

https://doi.org/10.5194/wes-2022-82
Preprint. Discussion started: 20 September 2022

eawe european academy of wind energy
Open Access WIND ENERGY SCIENCE DISCUSSIONS

$$\underset{\xi,\eta,u}{\text{maximize}}\ 8760\sum_{i=1}^{N}\sum_{j,k}\sum_{l=1}^{m+2} w_{jk}\eta_{ijk}^{l}p(u_{\mathrm{m}}^{l}) \tag{16a}$$

$$\text{subject to: } \xi_i+\xi_j\leq 1 \qquad \forall\, i,j\in \boldsymbol{N}_i \tag{16b}$$

$$n^{\min}\leq\sum_{j=1}^{N}\xi_j\leq n^{\max} \tag{16c}$$

$$\sum_{l=1}^{m+2}\eta_{ijk}^{l}u_{\mathrm{s}}^{l}\leq u_{ijk}\leq\sum_{l=1}^{m+2}\eta_{ijk}^{l}u_{\mathrm{h}}^{l} \qquad \forall\,(i,j,k) \tag{16d}$$

$$\sum_{l=1}^{m+2}\eta_{ijk}^{l}=1 \qquad \forall\,(i,j,k) \tag{16e}$$

$$u_{ijk}=u_{\infty}^{k}(\xi_i-\sum_{\ell\in\boldsymbol{U}_i^{\theta^j}}\xi_\ell\delta u_{i\ell}(\theta^j,u_{\infty}^{k})) \qquad \forall\,(i,j,k) \tag{16f}$$

$$\xi,\eta\in\{0,1\}\quad u\in\mathbb{R} \tag{16g}$$

The objective function in Eq. (16a) is an approximation of the AEP computation presented in Eq. (9). Equation (16b) models the minimum distance constraints as explained in the introduction of Sect. 3. If a binary variable ξ_i is active, then all candidate points closer than $d^{\min}$ should be excluded, i.e. set to zero. If a binary variable ξ_i is inactive then the other candidates are still eligible. The definition of the set $\boldsymbol{N}_i$ is provided in Eq. (11). Equation (16c) models the situation that the designer requires at least $n^{\min}$ and at most $n^{\max}$ WTs to be located in the domain. Note that for the classic problem definition $n^{\min}=n^{\max}$=n_{T}. Equation (16d) connects both state variables u and η as explained in Eq. (15). Eq. (16e) forces that there is one operation case active for each WT candidate at each wind direction and speed. The last constraint in Eq. (16f) is for the wake velocity deficit and wakes superposition modelling to calculate wind speed for each candidate location at each wind direction and inflow speed u_{∞}^{k}. The presented model supports a conservative velocity deficit approach (Eq. (3)) with linear superposition (Eq. (6)). The definition of set $\boldsymbol{U}_i^{\theta^j}$ is provided in Eq. (5). Note that an extension, consisting in creating extra continuous state variables and associated constraints, could allow for considering the more realistic approach in Eq. (4). It is still unknown if the root sum squares model of Eq. (7) could be implemented in the framework of MILP. Finally, Eq. (16f) defines the domain of the required variables. A value for u^{ini} of $u^{\text{cut-out}}$ is set up.

3.2 Power-curve-free model

Albeit the formulation of Sect. 3.1 succeeds at representing at a very good extent the physics ruling the problem, it has a considerable number of variables and constraints that may hinder the capacity to tackle interestingly sized problems. The next model that neglects power curve and AEP calculation is deployed, is intended to simplify it.

The model presented in this section deploys a strategy to account for the combination of Eq. (3) and Eq. (7) to calculate velocities, since the case studies from the IEA37 Wind Task 37 follow this outlook. It would be possible though to consider the linear superposition model if necessitated. However, this model does not support the application of Eq. (4).

https://doi.org/10.5194/wes-2022-82
Preprint. Discussion started: 20 September 2022

eawe european academy of wind energy
Open Access WIND ENERGY SCIENCE DISCUSSIONS

Combining Eq. (3) and Eq. (7) and extending the summation range in Eq. (7) to all candidate locations, the total wind speed in the farm, U, can be modelled through

$$U = \sum_{i=1}^{N} \sum_{j,k} w_{jk} u_{\infty}^{k} \xi_i - \sum_{i=1}^{N} \sum_{j,k} w_{jk} u_{\infty}^{k} \sqrt{\sum_{\ell=1}^{N} (\delta u_{i\ell}(\theta^j, u_{\infty}^{k}))^2 z_{i\ell}} \tag{17}$$

where new binary variables $z_{i\ell}$ are introduced. The variable $z_{i\ell}$ is equal to one if both WTs i and ℓ are active (i.e. if $\xi_i = \xi_\ell = 1$) and zero otherwise. Nevertheless, the previous expression is not linear for variable $z_{i\ell}$ due to the presence of the square root in each total relative velocity deficit term. Dropping the square roots, the following expression is obtained:

$$\tilde{U} = \overbrace{\sum_{i=1}^{N} \sum_{j,k} w_{jk} u_{\infty}^{k} \xi_i}^{\text{Total inflow wind speed}} - \overbrace{\sum_{i=1}^{N} \sum_{\ell=1}^{N} \sum_{j,k} w_{jk} u_{\infty}^{k} (\delta u_{i\ell}(\theta^j, u_{\infty}^{k}))^2 z_{i\ell}}^{\text{Total wind speed deficit proxy}} \tag{18}$$

Let the preprocessed coefficient in front of of $z_{i\ell}$ be

$$b_{i\ell} = \sum_{j,k} w_{jk} u_{\infty}^{k} (\delta u_{i\ell}(\theta^j, u_{\infty}^{k}))^2 \tag{19}$$

Combining Eq. (18) and Eq. (19) results in

$$\tilde{U} = \overbrace{\sum_{i=1}^{N} \sum_{j,k} w_{jk} u_{\infty}^{k} \xi_i}^{\text{Total inflow wind speed}} - \overbrace{\sum_{i=1}^{N} \sum_{\ell>i}^{N} (b_{i\ell} + b_{\ell i}) z_{i\ell}}^{\text{Total wind speed deficit proxy}} \tag{20}$$

Eq. (20) defines the objective function to be maximized of the power-curve-free model. In comparison to the objective function Eq. (16a), no power curve or continuous state variables are demanded.

Nonetheless, the presence of variables $z_{i\ell}$ can be troublesome. For the complete model, in addition to having these variables of combinatorial nature, constraints of the same kind must be incorporated: $z_{ij} \geq \xi_i + \xi_j - 1$, $z_{ij} - \xi_i$, $z_{ij} - \xi_j$. Experimental results show the heavy computational burden incurred when solving this formulation, impeding to solve large-scale problems (Fischetti et al., 2016). A big-M trick is then incorporated to come up with a model which is exactly equivalent, as reflected in formulation of Eq. (21).

https://doi.org/10.5194/wes-2022-82
Preprint. Discussion started: 20 September 2022

eawe european academy of wind energy
Open Access WIND ENERGY SCIENCE DISCUSSIONS

$$\underset{\xi,\tau}{\text{maximize}} \overbrace{\sum_{i=1}^{N}\sum_{j,k} w_{jk}u_{\infty}^{k}\xi_i}^{\text{Total inflow wind speed}} - \overbrace{\sum_{i=1}^{N}\tau_i}^{\text{Total wind speed deficit proxy}} \tag{21a}$$

$$\text{subject to: } \tau_i \geq \sum_{\ell=1:i\neq\ell}^{N} \xi_\ell b_{i\ell} + (\xi_i - 1)M_i \qquad \forall\, i \tag{21b}$$

$$n^{\min} \leq \sum_{i=1}^{N}\xi_i \leq n^{\max} \tag{21c}$$

$$\xi_i + \xi_j \leq 1 \qquad \forall\, i,j \in \boldsymbol{N}_i \tag{21d}$$

$$\xi \in \{0,1\} \quad \tau \in \mathbb{R} : \tau \geq 0 \tag{21e}$$

The new objective function in Eq. (21a) modifies the component linked to the total wind speed deficit proxy by creating variables τ_i; this variable means total wind speed deficit proxy for WT in candidate location i. Equation (21b) defines τ_i, if a WT candidate location is inactive $\xi_i = 0$, then there is no deficit at this location, therefore $\tau_i = 0$, because of $M_i = \sum_{\ell=1:i\neq\ell}^{N} b_{i\ell}$, and the minimization nature of the problem for wind speed deficits. Oppositely, if $\xi_i = 1$, then τ_i is forced to be equal to $\sum_{\ell=1:i\neq\ell}^{N} \xi_\ell b_{i\ell}$. The next two equations are the same with those already presented in Sect. 3.1 for number of active WTs, and minimum distance constraints. Finally, Eq. (21e) defines the domain of the required variables.

Note that for the classic problem definition $n^{\min} = n^{\max}$=n_{T}, the first part of the objective function becomes

$$\sum_{i=1}^{N}\sum_{j,k} w_{jk}u_{\infty}^{k}\xi_i = \sum_{j,k} w_{jk}u_{\infty}^{k}\sum_{i=1}^{N}\xi_i = \sum_{j,k} w_{jk}u_{\infty}^{k}n_{\mathrm{T}} = \text{constant}$$

For this situation, the objective function is thus equivalent to

$$\underset{\xi,\tau}{\text{minimize}} \sum_{i=1}^{N}\tau_i \tag{22}$$

4 Neighborhood Search Heuristic

In order to be able to address large-scale problems, a heuristic is proposed to wrap the previously presented MILP formulations in Sect. 3. It is based on neighborhood search and local branching theory (Fischetti and Lodi, 2003). The algorithm solves a sequence of MILPs, with different candidates number N or/and neighborhood search size K, taking advantage of robust and efficient implementations of branch-and-cut methods for MILP.

The heuristic relies on the observation that for a fixed layout described by $\xi \in \{0,1\}^N$, the other design and state variables are straight forward to determine. This observations is valid for all presented problem formulations in Sect. 3. Given $\xi \in \{0,1\}^N$, for the power-curve-based model, the continuous state variables u can be determined through classical wake analysis, and the

https://doi.org/10.5194/wes-2022-82
Preprint. Discussion started: 20 September 2022

eawe european academy of wind energy
Open Access WIND ENERGY SCIENCE DISCUSSIONS

binary state variables η are directly determined by inspection of the velocities. Similarly, for the power-curve-free model, the τ variables are trivially computed.

The pseudo code of the Neighborhood Search Heuristic (NSH) is described in detail in Algorithm 1.

Algorithm 1 Neighborhood Search Heuristic (NSH) Algorithm

$\boldsymbol{C} \leftarrow \{N_1, \cdots, N_C\}, N \in \boldsymbol{C}$ {**Input candidates set**}
$\boldsymbol{T} \leftarrow \{T_1, \cdots, T_C\}, T \in \boldsymbol{T}$ {**Input times set**}
$\boldsymbol{V} \leftarrow \{K_1, \cdots, K_V\}, K \in \boldsymbol{V}$ {**Input neighborhood sizes set**}
$countern \leftarrow 1 \quad counterv \leftarrow 1$
Obtain initial incumbent of activation binary variables for WTs ξ with objective value o_b
for $(\kappa = 1 : 1 : \kappa_{max})$ **do**
  $N \leftarrow \boldsymbol{C}[countern] \quad T \leftarrow \boldsymbol{T}[countern] \quad K \leftarrow \boldsymbol{V}[counterv]$
  Formulate optimization model with N candidates (including the incumbent), either from Sect. 3.1 or Sect. 3.2
  Add Hamming distance constraint centered around the incumbent ξ, $\sum_{i:\xi_i=0} \xi_i + \sum_{i:\xi_i=1}(1-\xi_i) \leq K$
  Solve opt. model from algorithm lines (8) to (9) until optimality or computing time T with ξ as warm-starter
  Get the solution pool $\mathbf{S}$, where $\hat{\xi} \in \mathbf{S}$ represents the activation binary variables for WTs of an individual solution
  *Apply **true objective function** over each solution $\hat{\xi} \in \mathbf{S}$, and obtain objective values set $\boldsymbol{O}$*
  Compute $o_t \leftarrow \max \boldsymbol{O}, and i_t \leftarrow \arg\max O$
  if $o_t > o_b$ **then**
    $o_b \leftarrow o_t$
    $\xi \leftarrow \mathbf{S}[i_t]$
  else
    $counterv \leftarrow counterv + 1$
  end if
  if $counterv = |\boldsymbol{V}| + 1$ **then**
    $counterv \leftarrow 1 \quad countern \leftarrow countern + 1$
  end if
  if $countern = |\boldsymbol{C}| + 1$ **then**
    Break
  end if
end for

The first three lines are for the main inputs of the algorithm: the candidates set $\boldsymbol{C}$, the times set $\boldsymbol{T}$, and neighborhood sizes set $\boldsymbol{V}$. The first set contains the sizes N of the meshes to be considered, the second one is for the maximum computing time T for the MILP solver for each size N, the last one is for the search size defined as the maximum number of changes K allowed to the incumbent solution.

https://doi.org/10.5194/wes-2022-82
Preprint. Discussion started: 20 September 2022

eawe european academy of wind energy
Open Access WIND ENERGY SCIENCE DISCUSSIONS

If the incumbent is improved, then the candidates set C, and neighborhood size K are kept, otherwise at least one of them is increased. The first step (line 5) is to obtain an initial incumbent binary variables, with the set ξ storing the acquired value (0 or 1) for each variable $\xi_i : i \leq N$. The incumbent has an objective value of o_b calculated after the ***true objective function***. The true objective function refers to the real equation that represents the ultimate aim to be optimized. For example, if this is the AEP, then it is the product of the power calculation process, applying the considered wake and superposition models and the original power curve, and not the objective function of the implemented formulation, as in Eq. (16a), which in any case is always an approximation.

The next step is to start the iterative process in line 6. Values for N, T, and K are fetched in line 7, followed by the formulation of the MILP model for candidates N accounting for the points of ξ. The Hamming distance, see e.g. (Fischetti and Lodi, 2003), centered around the incumbent point ξ, is added to the optimization model in line 9; this constraint reduces the search space as the number of changes to ξ are limited to K. The complete model is sent to the MILP solver with ξ as warm-starter, stopped until it reaches optimality or the assigned maximum computing time T.

After solver termination, the solution pool $\mathbf{S}$ is retrieved in line 11. It is very important to emphasize the aim of getting the whole pool instead of the best solution. This is done because of the imperfect correspondence between the true objective function and the objective function of the applied MILP model. For example, a solution which may have worse objective value, may actually have a better AEP according to the real model. In this order of ideas, the whole pool is examined, and the best solution indexed by i_t with AEP of o_t is obtained in line 13. If o_t is actually greater than o_b, then the whole algorithm is recentered around the new ξ (lines 14 to 16), and in the next iteration κ, the same values of N and K are maintained. Otherwise, the next value of K is taken (line 18), unless all of them have been traversed. In the last situation, the next candidates size N is considered given by $countern$, restarting the neighborhood set counter $counterv$ to one (lines 20 to 22). The NSH algorithm is terminated when all candidates set $\boldsymbol{C}$ have been processed (line 23 to 25).

5 Computational Experiments

As mentioned earlier in the manuscript, in order to have a transparent benchmark of the proposed methods, the open access case studies from the IEA37 Wind Task 37 (Baker et al., 2019; Dykes et al., 2015) are used for comparison. Those cases have circular project areas with three different radius (1300 m, 2000 m, and 3000 m) and number of WTs (16, 36, and 64), n_T. Thus, Case I has a radius of 1300 m and $n_\mathrm{T} = 16$ WTs, whereas Case II has radius 2000 m and $n_\mathrm{T} = 36$, and Case III has radius 3000 m and $n_\mathrm{T} = 64$, correspondingly.

The results of the statistical correlation between the proxy function given by the argument in Eq. (22), and AEP of the problem definition (Baker et al., 2019; Dykes et al., 2015) for each case are presented in Sect. 5.1. After this, the performances of the proposed models in the case studies are deployed in Sects. 5.2 (Case I), 5.3 (Case II), 5.4 (Case III). The power-curve-free model of Eq. (21) is implemented with the Eq. (22) as objective function. The true objective function in the NSH Algorithm 1 for these cases is the AEP of the problem definition. In the end, to prove the capabilities of power-curve-based model of Eq.

https://doi.org/10.5194/wes-2022-82
Preprint. Discussion started: 20 September 2022

(16), Sect. 5.5 displays results after applying this formulation with a modified objective function to express a metric similar to NPV.

The main parameters of the wake model in Sect. 2.1 are fixed to $C_T = 8/9$ and $k_y = 0.0324555$. Furthermore, a wind rose approach for modelling wind resource is utilized in this work. In a wind rose, the wind resource is binned in J directions, and for a specific direction j (θ^j), wind speeds are correspondingly discretized in V sectors. For the case studies, the wind rose is composed of 16 directions and a single wind speed k of 9.8 ms^{-1}. The considered wind rose is displayed in Fig. 2. Lastly, for the purpose of replicability of the numerical results, the power curve from Eq. (8) modelling the IEA37 3.35 MW reference turbine (with diameter of $D = 130$ m) is used in this manuscript (IEA Wind Task 37, 2019; Baker et al., 2019). The main parameters are $p^{\text{rated}} = 3.35$ MW, $u^{\text{rated}} = 9.8$ ms^{-1}, $u^{\text{cut-in}} = 4$ ms^{-1}, and $u^{\text{cut-out}} = 25$ ms^{-1}. The power curve for these specific parameter choices is plotted in Fig. 1.

The experiments for Sects. 5.2, 5.3, and 5.4 have been carried out on an Intel Core i7-6600U CPU running at 2.80 GHz with four logical processors and 16 GB of RAM. For the Sect. 5.5 a larger resource is used for being able to exploit the power-curve-based model capabilities, an Intel Xeon Gold 6226R CPU running at 2.90 GHz with 32 virtual cores and 640 GB of RAM.

The selected MILP solver is the commercial branch-and-cut algorithm implemented in IBM ILOG CPLEX Optimization Studio V20.1 (IBM, 2022). Some parameters are set to different values compared to the default choices. For example, the parameter emphasizing the finding of high-quality feasible solutions early in the process (`CPX_MIPEMPHASIS_HEURISTIC`) is activated. This is intended to generate more feasible layouts compared to the default setting which is important for the neighborhood search algorithm. Additionally, strong branching is used for variable selection given the large size of the models (`CPX_VARSEL_STRONG`). This setting is intended to reduce the size of the search tree and thus the memory requirements compared to default settings.

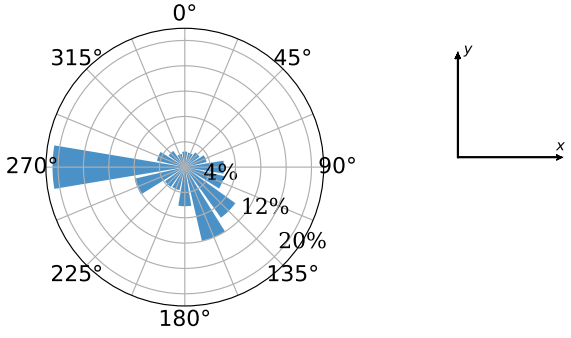

Figure 2. Wind rose used in the computational experiments. Taken from open access source (IEA Wind Task 37, 2019).

The number N and positions $\mathbf{p}_i$ for $i \leq N$ of the candidate locations are of course very important parameters for the adopted discrete modelling techniques. A customized automatic strategy has been employed based on independently sampling the

https://doi.org/10.5194/wes-2022-82
Preprint. Discussion started: 20 September 2022

eawe european academy of wind energy
Open Access WIND ENERGY SCIENCE DISCUSSIONS

boundary and interior area of the circular domain $\mathbf{F}$. An example of the sampling strategy for these particular case studies giving $N = 467$ is illustrated in Fig. 3.

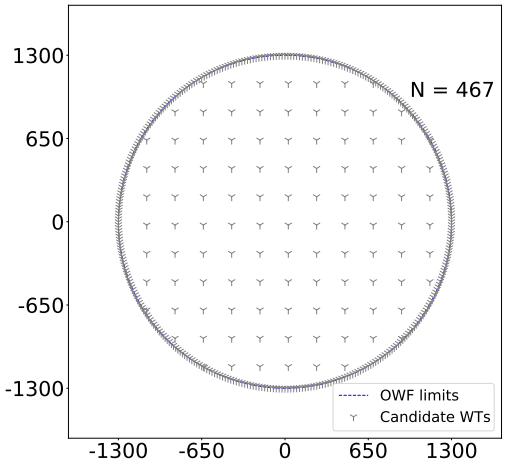

Figure 3. Example of generation of WTs candidate locations N.

In the above figure is noticeable that the boundary is densely sampled, as a candidate point is defined every natural angle from $0°$ to $359°$, i.e. 360 candidate points are provided. This is done as it is intuitively expected that a good portion of the WTs will be placed in the boundaries, as WTs will be spread out in the available area as much as possible to decrease wake losses. For the interior, a set of finite parallel line segments are generated in between of the extreme abscissa and ordinate points of the available project area. The candidates points are then taken along those segments, according to sampling parameters, such as, distance between the points along a line, and vertical distance between lines. In the example of Fig. 3, the slope of the line segments is zero, and the distance between points and lines is equal to $1.7D$. Although in this example a circle with radius of 1300 m is displayed, the underlying principles apply for any project area shape.

5.1 Correlations

To validate the approach modelled by the MILP formulation of Eq. (21) (i.e. the power-curve-free model), 5000 random feasible WT layouts are created. For each of them, the AEP (Baker et al., 2019; Dykes et al., 2015), the total wind speed theoretical, U, given by Eq. (17), the total wind speed proxy, $\tilde{U}$, defined by Eq. (20), and total wind speed deficit proxy, $\sum_{i=1}^{N} \tau_i$, argument of Eq. (22), are calculated. Although the random way of generating the layouts biases the obtention of high-quality solutions, the general trend is the aspect of interest and can be assumed to be fairly representative for the whole domain.

In all cases Pearson product-moment linear correlation coefficients (Pearson, 1895) are used to extract information from the data, the results are collected in Table 1 for every single pair of the aforementioned measures. This coefficient illustrates the degree to which the movement of pairs of variables is associated in a linear fashion. The correlation plots of Fig. 4 present the graphical representation of the relations for Case I.

https://doi.org/10.5194/wes-2022-82
Preprint. Discussion started: 20 September 2022

eawe european academy of wind energy
Open Access WIND ENERGY SCIENCE DISCUSSIONS

The correlation between AEP and the total theoretical wind speed is shown in Fig. 4a for the Case I. The main observation is the very strong linear relation between these two variables as illustrated by the correlation coefficient of 0.97. Interestingly, this reflects the rather low influence of the WT power curve to determine high-quality feasible points. The next observation is present in Fig. 4b. In this plot, the relation between U and $\tilde{U}$ is represented, resulting in almost an identical linear connection between them, as in the previous graph. When one looks into AEP vs $\sum_{i=1}^{N} \tau_i$, however, it is noticeable that the Pearson coefficient worsens, decreasing to -0.88. There is a wider area in the formed body of points that causes this behaviour. Note that in contrast to the previous two figures, there is a negative correlation because the comparison is done in terms of wind speed deficit instead of total wind speed. In spite of this deterioration, the linear correlation is still strong enough. These results motivate an approach where the minimization of a proxy total wind speed deficit can lead to high-quality AEP solutions. The NSH Algorithm 1 helps correcting the imperfect correspondence between these two variables during the optimization routine as reflected in Sect. 4.

For Case II the general trends of the correlation plots are very similar to the observed in the previous case. Correlations between AEP versus total wind speed theoretical (0.97), and total wind speed theoretical versus total wind speed proxy (0.95) are still very strong. Nonetheless, there is a slight worsening between the relation of AEP vs total wind speed proxy (it moved from -0.88 in the previous case to -0.85), as the spread for middle velocity values is enlarged. The linear relation is deemed as satisfactory enough to carry on with the application of model of Eq. (21).

Lastly, for Case III yet another very strong the linear relation between AEP and the total wind speed theoretical (0.96) is observed, just as for the two previous situations. This is a very interesting outcome of this manuscript. Almost all research in the WFLO problem strictly focuses in power modelling, which brings a great deal in complexity due to the non-linear and non-differentiable properties of a typical WT power curve. Using an exact model for determining total wind speed as objective function alleviates the computational complexity, while being able to find high-quality solutions in terms of AEP for the classic WFLO problem.

Nevertheless, deterioration in the correlations stemming from the proxy to calculate total wind speed deficit is present in this case. Both with the total wind speed theoretical (0.88) and the AEP (-0.72). Keep in mind that the reason to formulate such approximation is to fit in the context of integer programming to leverage theory and state-of-the-art algorithms of this mature field by having a compact formulation. However, the price to pay is to lose fidelity to represent the real (true) target to optimize. The deterioration in the correlation of these pairs of variables may also suggest the need to resort to the power-curve-based model for some applications. Whether the price is too high or not is reflected in the reachable solution quality. Sects. 5.2, 5.3, and 5.4 present the optimization results for the cases of fixed number of WTs that will ultimately help to elaborate a final evaluation regarding the adopted modelling technique.

https://doi.org/10.5194/wes-2022-82
Preprint. Discussion started: 20 September 2022

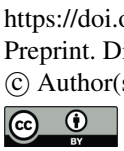

eawe european academy of wind energy
Open Access WIND ENERGY SCIENCE DISCUSSIONS

Table 1. Pearson product-moment linear correlation coefficients for all case studies.

Case	AEP vs Theoretical wind speed	Theoretical vs Proxy wind speed	AEP vs Proxy wind speed deficit
Case I	0.97	0.96	-0.88
Case II	0.97	0.95	-0.85
Case III	0.96	0.88	-0.72

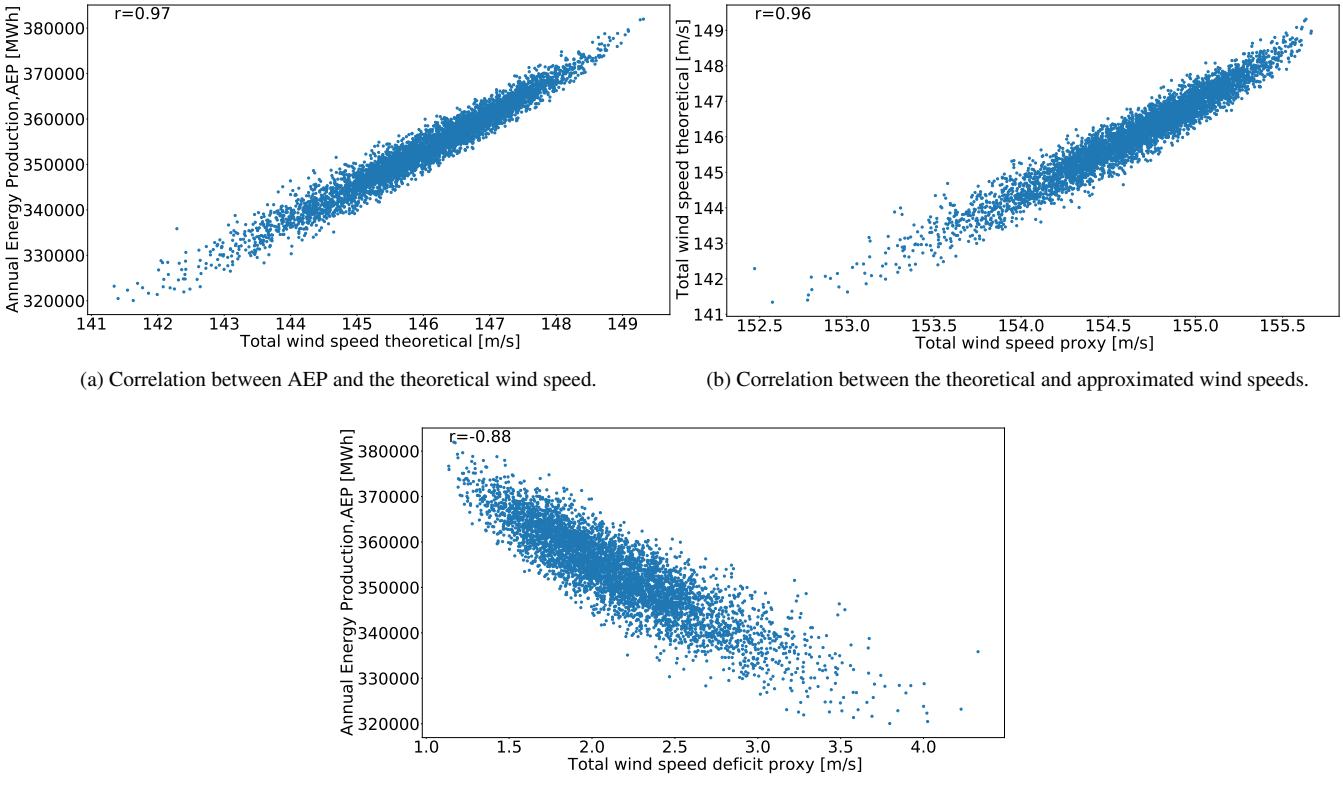

(a) Correlation between AEP and the theoretical wind speed.

(b) Correlation between the theoretical and approximated wind speeds.

(c) Correlation between AEP and the approximated wind speed deficit.

Figure 4. Correlation plots for 5000 randomly generated wind turbine layouts for Case I.

5.2 Case I: 16 WTs

The performance evolution of two of the proposed optimization frameworks in this article is depicted in Fig. 5. The green line of the full model is obtained after solving the model of Eq. (21) with objective function as in Eq. (22) for $N = 1014$ without implementing the NSH. In order to plot this line, the CPLEX's log is postprocessed by finding out the incumbent solution in terms of AEP and not for total wind speed deficit proxy. The blue line results after applying the NSH with the model of Eq. (21) plus objective Eq. (22), and AEP as true objective function in Algorithm 1. The main inputs are $\boldsymbol{C} = \{467, 590, 1014\}$,

https://doi.org/10.5194/wes-2022-82
Preprint. Discussion started: 20 September 2022

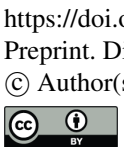

eawe european academy of wind energy
Open Access WIND ENERGY SCIENCE DISCUSSIONS

$\boldsymbol{T} = \{1, 1.5, 2\}$ h, $\boldsymbol{V} = \{2, 4, 6, 16\}$. These inputs are tuned after evaluating the performance of the method using different values. In general, the first two elements of $\boldsymbol{C}$ consists of moderately big values, relatively close to each other, while the last element is sizeably greater in the seek of the best possible solution. Each element $N \in \boldsymbol{C}$ has associated a computing time T. Finally, the first elements of $\boldsymbol{V}$ are relatively low values to favour termination of the solver due to optimality, and then they start increasing to refine the search. The red line is for establishing a reference of AEP value, this comes from the best performing method in the survey of IEA37 Wind Task 37 (Baker et al., 2019), the SNOPT plus Wake Expansion Continuity (WEC) (Thomas and Ning, 2018; Thomas et al., 2022b). Time evolution for the SNOPT+WEC is not reflected in this graph, as this information is unavailable. Results for the benchmark against a testbed of different algorithms are available in Table 2.

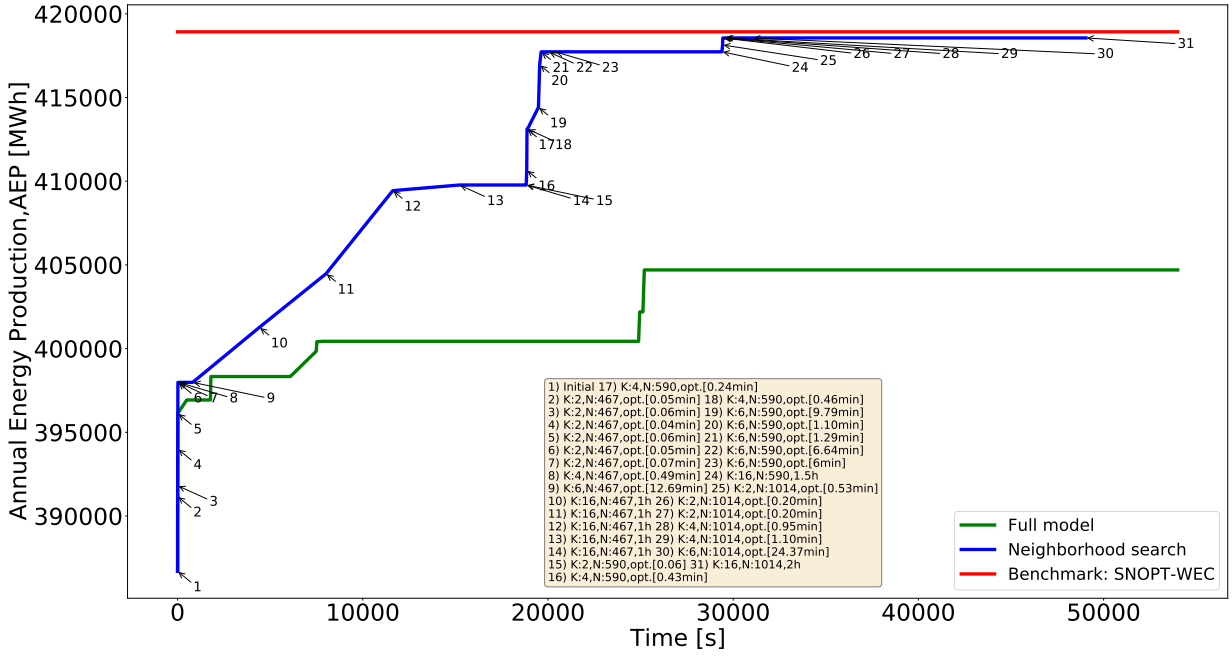

Figure 5. Performance of two different optimization approaches for Case I and comparison with existing best benchmark results.

The yellow box in Fig. 5 contains information about the values of N, T, and termination criterion of the solver after each iteration κ of the NSH Algorithm 1 (beginning from point 2 where $\kappa = 1$). The initial layout (point 1), which is graphed in Fig. 6a, is set up by arbitrarily picking up candidate locations around the circular boundary; this layout has an AEP of 86699 MWh. Between points 2 to 6 where $N = 467$ and $K = 2$, the models are solved to optimality (gap of 0%), and the solution is improved by 2.92% in only 56 s. After a short plateau, the solution is markedly refined by 2.96% from point 10 to 13 by performing a full search of the domain ($K = 16$), and restarting the model every 1 h with a new warm-starting. The percentages are calculated with respect to the last commented improvement.

The next considerable jump happens for $N = 590$ and $2 \leq K \leq 6$ in around 20 min, elevating the AEP by 1.94%. After, again, a plateau without improvements, when N reaches its maximum value of 1014, the solution is maximized to the final

https://doi.org/10.5194/wes-2022-82
Preprint. Discussion started: 20 September 2022

eawe european academy of wind energy
Open Access WIND ENERGY SCIENCE DISCUSSIONS

value of 418559.44 MWh during the lowest values of K. For this particular instance, the greatest value of $K = 16$ is exploited for the lowest number of candidate points N, where the largest improvement comes up.

Table 2. Results for all three benchmark cases from other algorithms (G, gradient-based and GF, gradient-free) obtained while allowing turbine locations to vary continuously. The AEP values for each case/algorithm in GWh are reproduced from the IEA37 study (Baker et al., 2019). The difference column shows how the proposed heuristic with the power-curve-free model performs in comparison in %. Negative percentages means that the proposed method performs better than the corresponding algorithm.

Method	AEP I	Diff. I	AEP II	Diff. II	AEP III	Diff. III
SNOPT+WEC (G)	418.92	0.09	863.68	-0.19	1513.31	0.85
fmincon (G)	414.14	-1.06	820.39	-5.19	1336.16	-10.95
SNOPT (G)	412.25	-1.51	846.36	-2.19	1476.69	-1.59
SNOPT (G)	411.18	-1.76	844.28	-2.43	1445.97	-3.64
Preconditioned SQP (G)	409.69	-2.12	849.37	-1.84	1506.39	0.39
Mul.interior-point (G)	408.36	-2.44	851.63	-1.58	1480.85	-1.31
Full pseudo-gradient (GF)	402.32	-3.88	828.75	-4.23	1455.08	-3.03
Basic genetic algorithm (GF)	392.59	-6.20	777.48	-10.15	1332.88	-11.17
Simple particle swarm (GF)	388.76	-7.12	776	-10.32	1364.94	-9.04
Simple pseudo-gradient (GF)	388.34	-7.22	813.54	-5.98	1422.27	-5.22

The benefit of the proposed neighborhood search strategy is shown in Fig. 5. Solving the full model is significantly slower, leading actually to a worse solution (3.31% lower). The capacity of the NSH to iterate over different values of candidate points N and search size K brings alone not only improvements in terms of solution time and solution quality, but also in less computational resources as the RAM memory generally escalates faster when solving the single model.

The initial and final solution layouts for this case study are illustrated in Fig. 6. The importance of finely sampling the boundaries of the available area is evident in Fig. 6b, because 7 out of the 16 WTs are placed in that subdomain.

Finally, Table 2 compares the proposed method to a large number of different approaches from the IEA37 reference study (Baker et al., 2019). The results for all case studies are presented in this table, where I, II, and III make reference to cases from this section, Sect. 5.3, and Sect. 5.4, respectively. For details of each of the benchmark algorithms, the reader is referred to the mentioned reference.

The third column of Table 2 reports the difference of the AEP with respect to the proposed method for the smallest case study. The obtained AEP in this case is better than almost all the other alternatives, except to the SNOPT+WEC, where a nearly identical objective value is achieved. When directly comparing to the gradient-free (GF) methods, the best found solution by them (full pseudo-gradient with 402318.75 MWh) is determined in around 2 h by the proposed method, which is typically way faster than the overall performing computing time of these kind of algorithms. Discrete optimization approaches, as the

https://doi.org/10.5194/wes-2022-82
Preprint. Discussion started: 20 September 2022

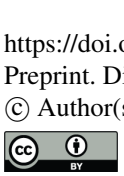

eawe european academy of wind energy
Open Access WIND ENERGY SCIENCE DISCUSSIONS

MILP ones presented in this article, could be formulated to cope with problem definitions with required functionalities that in theory continuous optimization methods can not support (or at least the implementation becomes strenuous).

The power-curve-based model of Eq. (16) within the NSH using the same AEP formulation as true objective function, provides a solution 1.18% lower in objective value in around 36 h using the computer system with 32 virtual cores. Although the quality of the layout is very close to the one schematized in Fig. 6b, the need for larger computational resources tips the scales for implementing the power-curve-free model for these type of problems with fixed number of WTs. For this reason, in Sects. 5.3 and 5.4 are presented only the results reached after the application of the power-curve-free model embedded into the NSH.

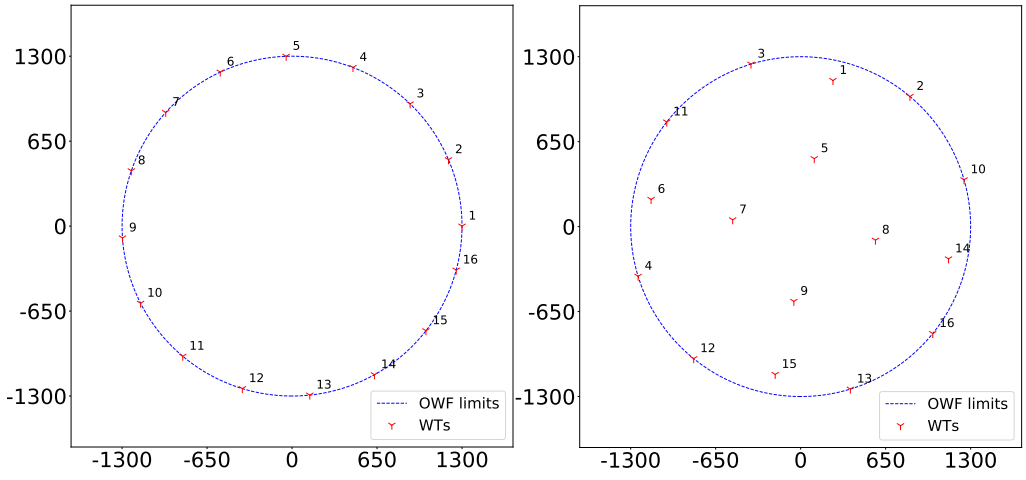

(a) Initial wind farm layout provided to the heuristic. (b) Final wind farm layout obtained by the heuristic.

Figure 6. Generated wind farm layouts for the benchmark Case I with 16 turbines.

5.3 Case II: 36 WTs

The performance evolution of the proposed methods, and the initial and final WT layouts are plotted in Fig. 7 and Fig. 8, respectively. Main inputs are $\boldsymbol{C} = \{477, 684, 1907\}$, $\boldsymbol{T} = \{1, 1.5, 2\}$ h, $\boldsymbol{V} = \{2, 4, 8, 16, 36\}$. The blue line (model of Eq. (21) with objective function Eq. (22) plus NSH Algorithm 1) has clearly three sectors stemming from each value of $N \in \boldsymbol{C}$. The initial WT layout (Fig. 8a) - also determined by choosing roughly equidistant candidate locations in the boundary - has an AEP of 796514.61 MWh. After seven iterations of the NSH (point 8) in 41 s, the incumbent is improved by 1.84%, when $N = 477$ and $2 \leq K \leq 4$, being able to solve each model instantation to optimality.

As shown in Fig. 7, after a three-hours-plateau linked to $8 \leq K \leq 36$ (four iterations), N is raised to 684, resulting in the sharpest AEP enhancement. The energy production increases with 4.51% after only 23 min in point 27. This noticeable improvement comes after solving to optimality models with rather small neighborhood search sizes $2 \leq K \leq 4$. The convenience of allowing large neighborhood search sizes as $K = 16$ or $K = 36$ is reflected from this moment. From point 30 to 33 (6 h) with $K = 16$ the incumbent is slowly boosted by nearly 1%. Again, after a three-hours-plateau, N becomes equal to 1907, and

https://doi.org/10.5194/wes-2022-82
Preprint. Discussion started: 20 September 2022

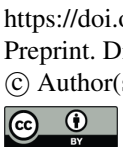

eawe european academy of wind energy
Open Access WIND ENERGY SCIENCE DISCUSSIONS

in around 32 min for $2 \leq K \leq 4$, the AEP is augmented by 0.41%. Then, the large neighborhood search starts for $K = 16$ and $K = 36$, and after a total of 16 h, the final solution of 865327.78 MWh (increment of 0.61%) is achieved (Fig. 8b).

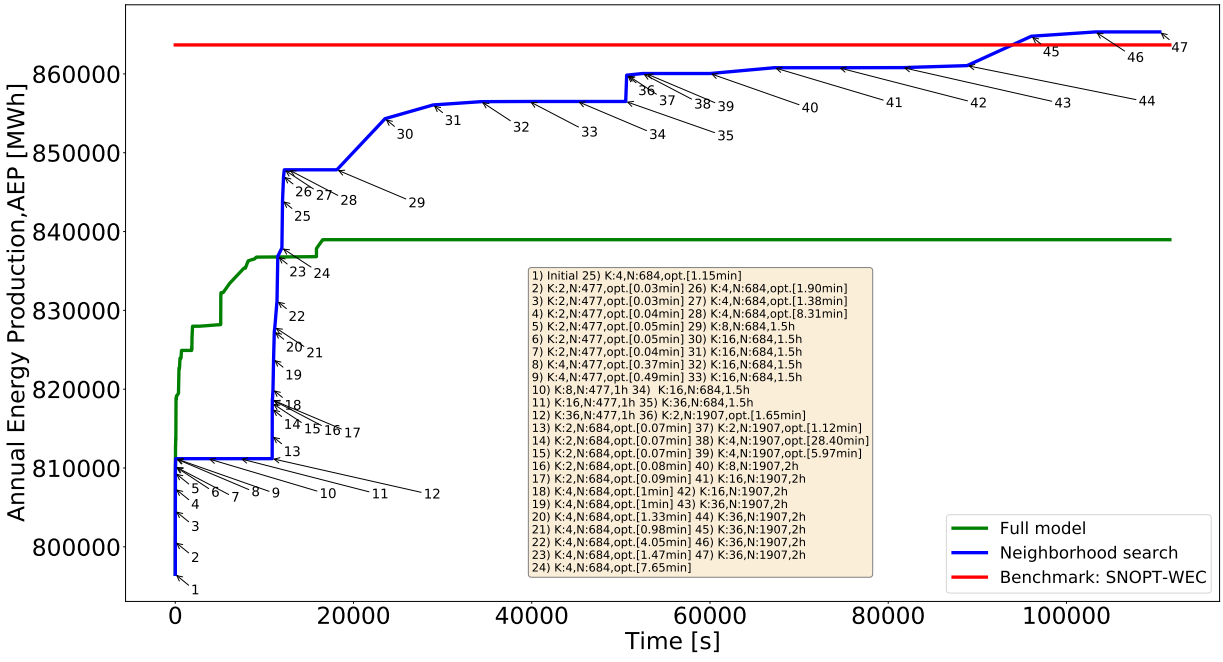

Figure 7. Performance of two different optimization approaches for Case II and comparison with existing best benchmark results.

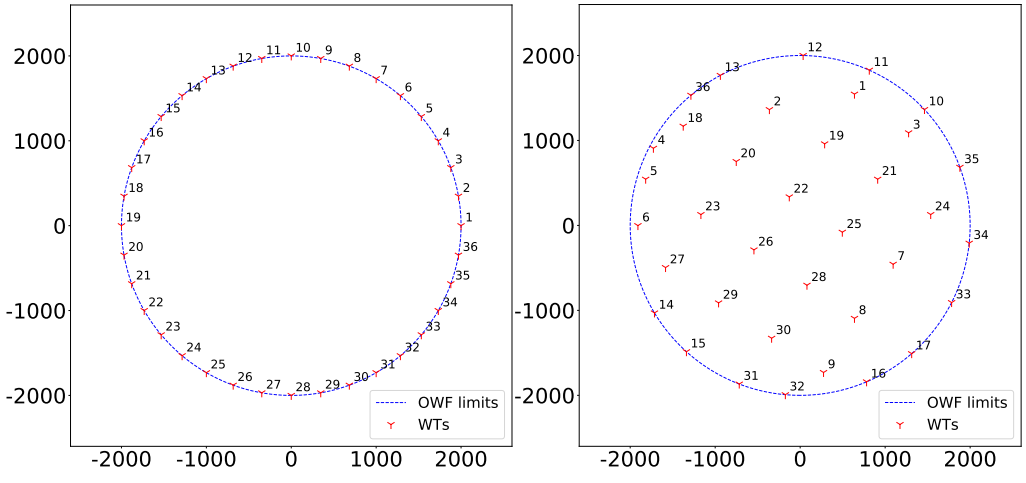

(a) Initial wind farm layout provided to the heuristic. (b) Final wind farm layout obtained by the heuristic.

Figure 8. Generated wind farm layouts for the benchmark Case II with 36 wind turbines.

https://doi.org/10.5194/wes-2022-82
Preprint. Discussion started: 20 September 2022

eawe european academy of wind energy
Open Access WIND ENERGY SCIENCE DISCUSSIONS

At this point is possible to establish a pattern in the operation of the NSH algorithm. Small neighborhood search sizes result in the fastest enhancement of the objective function, but large neighborhood search is very important as a slow cook refinement for reaching the final high-quality solutions.

Opposed to Fig. 5, in Fig. 7 is distinguishable that the full model (i.e. without implement the NSH algorithm) initially provides better solutions within the first 3 h, but then it remains in a considerably worst solution than when applying the NSH algorithm in the long run (lower 3.05%).

In this case, the proposed method reaches the best solution, as given in the fifth column of Table 2. The SNOPT+WEC is again the closest contender. When uniquely comparing to GF methods, the proposed method matches the best solution from those algorithms in around 3 h, which is generally a very fast computing time when contrasted to other methods where gradients are not explicitly utilized in the optimization process.

5.4 Case III: 64 WTs

The performance evolution of the proposed methods, and the initial and final WT layouts are displayed in Fig. 9 and Fig. 10, respectively. Main inputs are $\boldsymbol{C} = \{625, 1017, 2741\}$, $\boldsymbol{T} = \{1, 1.5, 2\}$ h, $\boldsymbol{V} = \{2, 4, 8, 16, 32, 64\}$. Note that in comparison the number of elements of $\boldsymbol{V}$ has been increased by one after each study case. This has been done taking into account the number of WTs. Likewise, the values of $N \in \boldsymbol{C}$ are greater to cover for the wider project areas.

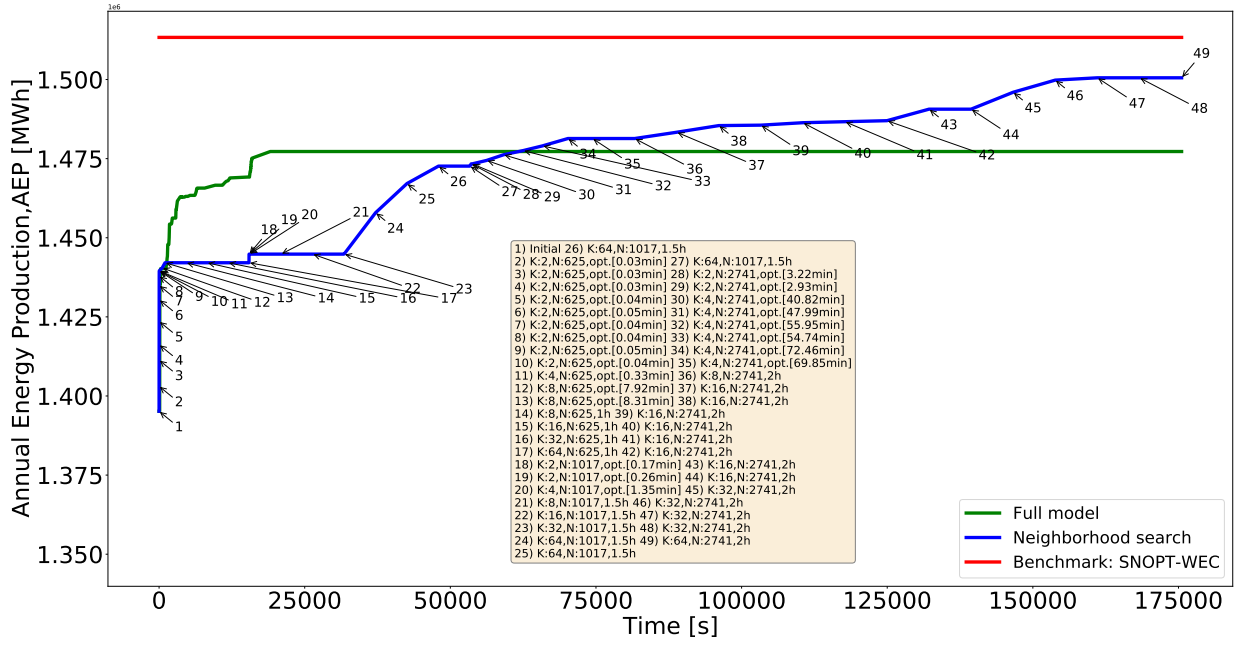

Figure 9. Performance of two different optimization approaches for Case III and comparison with existing best benchmark results.

Comparing blue lines of Fig. 6, Fig. 8, and Fig. 10 is evident that for the last case the curve shows less sudden increases. The sharpest change is after the first 27 s where the initial solution (Fig. 10a) with AEP of 1395165.92 MWh is improved by

https://doi.org/10.5194/wes-2022-82
Preprint. Discussion started: 20 September 2022

eawe european academy of wind energy
Open Access WIND ENERGY SCIENCE DISCUSSIONS

3.18% for $N = 625$ and $K = 2$ up to point 9, reaching optimality in few seconds. With $4 \leq K \leq 8$ the model instantiations are solved to optimality in minutes, obtaining a solution improved by 0.18%.

After point 13 a plateau without improvement proceeds for $N = 625$ and $K \geq 16$, i.e., a large neighborhood search does not lead to further enhancements. Due to this, N is enlarged to 1017, where the total second largest boost (increase of 2.12%) comes, being the full search ($K = 64$) particularly fruitful, as in this instantiation brings along the best improvement. This enhacement occurs after 13 h of starting the NSH (point 26). Next from point 28, $N = 2741$ and for $2 \leq K \leq 4$ the solver reaches optimality; the following greater neighborhood search sizes permit for a very slow evolution to finally converge to the final solution of 1500544.26 MWh (Fig. 10b).

Seventh column of Table 2 shows that the SNOPT+WEC and the preconditioned SQP provide slightly better layouts than the proposed method for this case. However, the algorithm provides feasible layouts that improve the objective compared to all the listed gradient-free approaches.

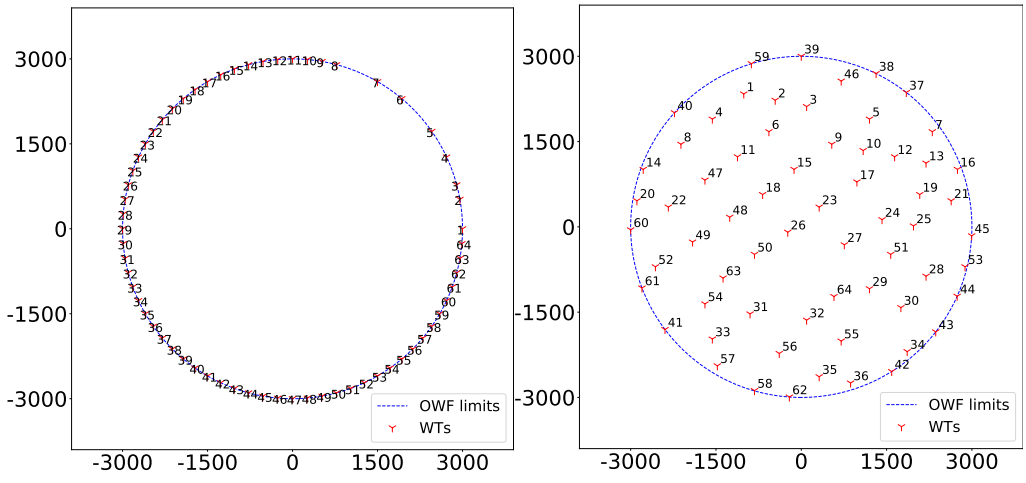

(a) Initial wind farm layout provided to the heuristic. (b) Final wind farm layout proposed by the heuristic.

Figure 10. Generated wind farm layouts for benchmark Case III with 64 wind turbines.

5.5 Case IV: 10-50 WTs

Although in most projects today the total capacity for grid connection is decided already in the early planning phases, in the future one can envisage situations where flexibility in optimizing the number of wind turbines in a project would yield benefits.

As much as the power-curve-free model presented in Sect. 3.2 exhibits a quite good performance both in terms of AEP and computing time for the scenario of fixed number of WTs, it is not very well suited for optimizations aiming at improving economic indices, like NPV. For such an optimization, the power-curve-based mathematical program of Sect. 3.1 may be handy as the number of generators is allowed to vary between a lower and upper bound, $n^{\min}$ and $n^{\max}$, respectively. For illustration, a domain defined by a circle with radius 1300 m, and variable number of WTs between 10 and 50 are utilized. These parameters are set relatively arbitrarily but with sufficient distance to reasonably expect that the limits are not reached.

https://doi.org/10.5194/wes-2022-82
Preprint. Discussion started: 20 September 2022

eawe european academy of wind energy
Open Access WIND ENERGY SCIENCE DISCUSSIONS

The aim is to illustrate the ability of the method in reaching non-trivial solutions, resulting in a an optimized design with an an intermediate number of wind turbines.

Keep in mind that for this case, a linear superposition model for the AEP component in the NPV calculation is considered. In this sense, the original WT power curve as deployed in Fig. 1 is supported. NPV is the true objective function when applying the NSH Algorithm 1. The modified objective function of MILP model of Eq. (16) for this case has the form (Investopedia, 2022):

$$\underset{\xi,\eta,u}{\text{maximize}} \; -\sum_{i=1}^{N} c_{\text{wt}}\xi_i + 8760 \sum_{y=1}^{Y} \sum_{i=1}^{N} \sum_{j,k} \sum_{l=1}^{m+2} \frac{c_{\text{e}} w_{jk} \eta_{ijk}^{l} p(u_{\text{m}}^{l})}{(1+r)^{y}} \tag{23}$$

where c_{wt} is the cost per WT in Mill.Eur, c_{e} the energy price in Mill.EurMWh^{-1}, r is the discount rate in %, and Y is the number of years of lifetime of the project. For this case study, values of $c_{\text{wt}} = 6.7$ Mill. Eur (Nord Pool, 2022), $c_{\text{e}} = 0.00015$ Mill.EurMWh^{-1} (Mishnaevsky Jr and Thomsen, 2020), $r = 5\%$, and $Y = 20$ are assumed.

Three runs launching the model of Eq. (16) with modified objective function Eq. (23), embedded in the NSH Algorithm 1 with NPV as target function are executed. For the first example the number of turbines is fixed to $n^{\min} = n^{\max} = 10$. In the second example the number of turbines remains fixed but is increased to $n^{\min} = n^{\max} = 50$. For the final example the number of wind turbines are allowd to vary between $n^{\min} = 10$ and $n^{\max} = 50$. The inputs parameters for Algorithm 1 are $\boldsymbol{C} = \{467, 590, 1014\}$, $\boldsymbol{T} = \{1, 1.5, 2\}$ h, $\boldsymbol{V} = \{2, 4, 6, 8, 24\}$. The main results are plotted in Figures 11, 12, and 13, respectively.

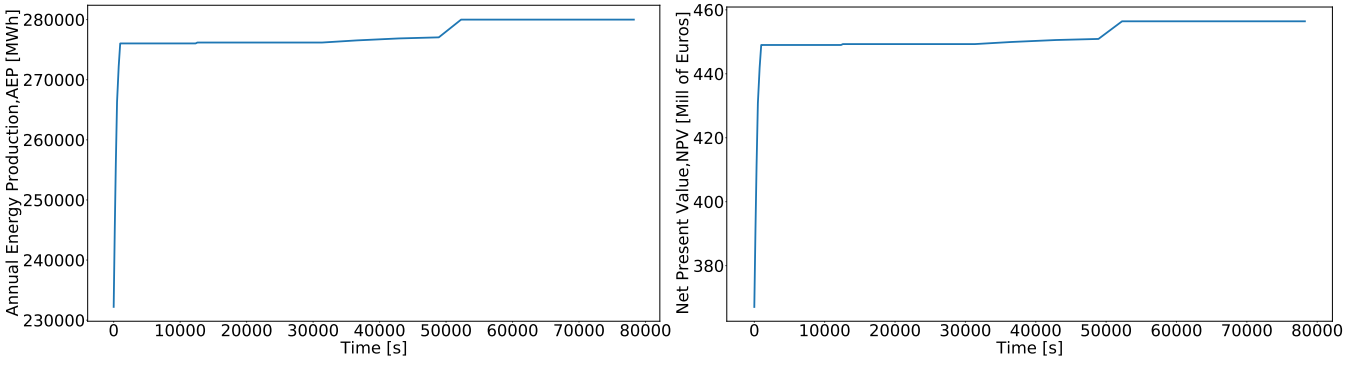

(a) AEP evolution.

(b) NPV evolution.

Figure 11. Evolution of the AEP and NPV with number of wind turbines fixed to 10 applying the power-curve-based model.

https://doi.org/10.5194/wes-2022-82
Preprint. Discussion started: 20 September 2022

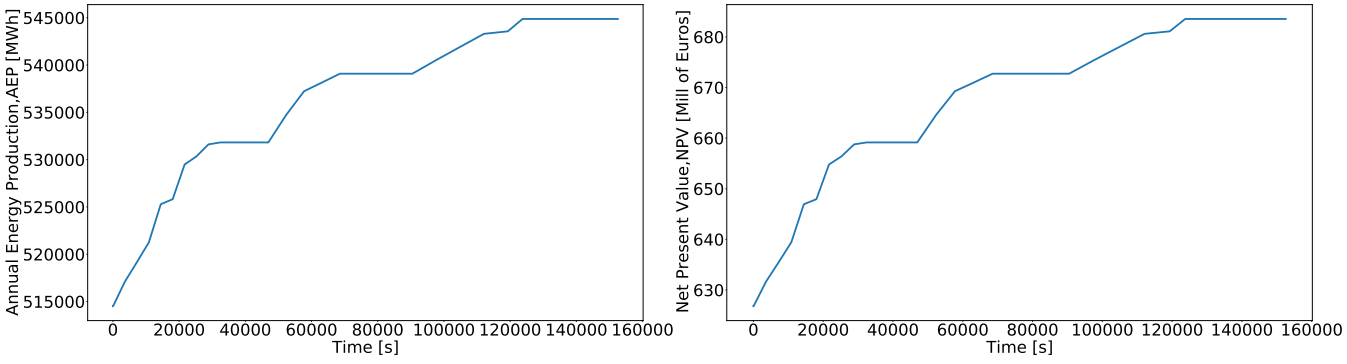

(a) AEP evolution.

(b) NPV evolution.

Figure 12. Evolution of the AEP and NPV with number of wind turbines fixed to 50 applying the power-curve-based model.

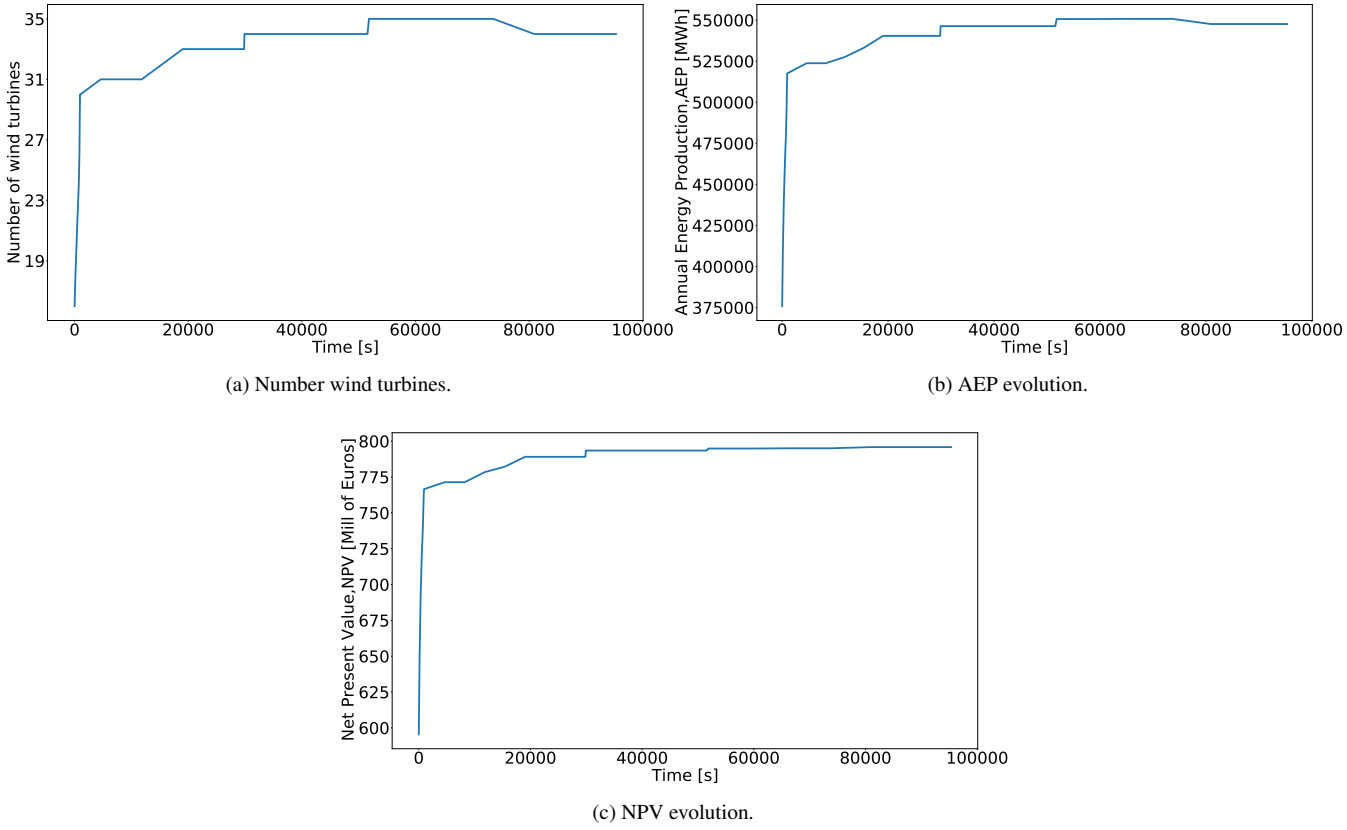

(a) Number wind turbines.

(b) AEP evolution.

(c) NPV evolution.

Figure 13. Evolution of the AEP and NPV with variable number of wind turbines between 10 and 50 applying the power-curve-based model.

When the number of turbines is fixed to 10, the NPV evolution (Fig. 11b) is driven by the AEP (Fig. 11a). Both curves are monotonically increasing, reaching a final value of NPV of $= 456.40$ Mill. Eur. The same behaviour is visible for $n_T = 50$,

https://doi.org/10.5194/wes-2022-82
Preprint. Discussion started: 20 September 2022

eawe european academy of wind energy
Open Access WIND ENERGY SCIENCE DISCUSSIONS

although the final NPV is greater (683.53 Mill. Eur), see Figure 12. The difference in discounted cash flow revenues surpasses the associated extra investment costs from the additional number of wind turbines.

Whether there is a trade-off point in between of both extreme cases is the main question to answer. The evolution of the WTs number in Fig. 13a and the AEP in Fig. 13b exhibits a perfect correspondence. The more WTs the larger AEP, in spite of the increased wake losses. The curves increase in time, up to a point where the model estimates that further increase of WTs would not lead to a better NPV. The final number of WTs is 34. The NPV evolution in Fig. 13c naturally only improves with time, resulting in a final value of 795.86 Mill. Eur. Note that the NPV in this case is greater than when a larger number of WTs (i.e. 50) was considered and of course when only 10 were considered.

This result shows the benefit of having optimization models that support variable number of WTs accounting for metrics beyond AEP. The advantages may become even more pronounced for more complex situations, as for instance, if the WT investment costs are dependent on the exact installation area or different WT sizes are considered.

6 Discussions and future work

The two models proposed in this article have many of the common characteristics of mixed integer linear programming models. They require significant resources like computational time and memory. Furthermore, they exhibit rather low tractability and scalability for global optimization algorithms.

The power-curve-based model, albeit requiring large computational resources as number of cores and RAM memory, manages to provide reasonably good solutions for small-sized problem instances, being only 1.18% worse than its power-curve-free counterpart for the 16 WTs case and 4.41% for the 36 WTs case. This diminishing effectivity is to be expected, given the large number of variables and constraints. The power-curve-free model on the other hand along with the heuristic is much faster due to its associated more compact formulation. This translates into the ability to be highly competitive compared to a large set of benchmark algorithms. In situations where there is an interest for optimizing metrics beyond AEP, such as the NPV, the power-curve-based model becomes very useful given its intrinsic capacity to support this kind of objective functions, as shown in the final test case.

It is relevant to mention that there are limitations in the used wake models compared to recent models from the literature (Thomas et al., 2022b). For example, the used wake model does not consider the modifications of the turbulence intensity or thrust coefficient variations from wind speed inside the wind farm. It is uncertain if these modifications would still allow an integer linear programming formulation or approximation of the WFLO problem. It is also uncertain what impact on the final solution quality these detailed modelling aspects imply. These questions are left for future work.

Notwithstanding the listed shortcomings, it is very enthralling that these models in combination with the neighborhood search heuristic are able to match and in some cases improve the results obtained when considering the turbine positions as continuous variables (see Table 2). This opens the door to trying out new case studies with functionalities easily adaptable to discrete parametrization techniques, which can be very challenging for continuous variable modelling approaches.

https://doi.org/10.5194/wes-2022-82
Preprint. Discussion started: 20 September 2022

Future work can include the application of the proposed methods to real-world problem instances with for example, forbidden areas, complex turbine cost functions or integrated optimization with electrical systems. Furthermore, the assessment of the robustness of the method for different initial layouts can be assessed in following studies.

7 Conclusions

This manuscript contributes both methodologically and empirically to address the WFLO problem. It is very difficult to cope with extended versions of the classic problem definition. Relevant extensions include variable number of WTs or complex forbidden areas. For these situations there is a need to develop new modeling and algorithmic approaches in this direction. A neighborhood search heuristic embedding integer programming formulations is therefore proposed to satisfy these new demands. For both presented formulations, the step-wise power curve and power-curve-free, the heuristic notably improves a single execution of full models when calling a state-of-the-art branch-and-cut solver in terms of solution quality. An improvement of up to 3.42% in the AEP is achieved by applying the neighborhood search strategy for cases where the WTs number is fixed compared to solving the full model.

Another important takeaway is the satisfactory performance of the power-curve-free model, which uses an approximation of the total wind speed deficit, when (implicitly) optimizing for AEP. This is due to the good correlation between the two measures, and the correction capability of the heuristic. For the classic WFLO problem definition, the proposed model is able to considerably enhance (from 1% to around 10%) the AEP compared to benchmark layouts obtained by several different gradient-based and gradient-free algorithms. Even when directly compared to methods implementing a continuous variables technique, the proposed heuristic provides very competitive results, being able to come up with layouts with similar objective function values, or even improving it. These are very promising results that would enable to get high-quality solutions for problem instances where continuous variables modelling approaches may not be able to run or come up with good incumbents.

Finally, the model with explicit representation of the power curve embedded within the neighborhood search heuristic is able to propose non-trivial solutions when implementing an objective function beyond AEP, such as NPV. For these cases the trade-off between energy revenues and investment costs is inherently studied. For the case study, the model suggests that is not worth to install the maximum number of allowed wind turbines, but a lower value that reflects a better NPV value.

Author contributions. Juan-Andrés Pérez-Rúa: Conceptualization, Methodology, Software, Validation, Formal analysis, Data Curation, Writing. Mathias Stolpe: Conceptualization, Methodology, Investigation, Resources, Supervision. Nicolaos A. Cutululis: Validation, Writing, Supervision, Project administration, Funding acquisition.

Competing interests. Nicolaos A. Cutululis is a member of the editorial board of Wind Energy Science.

https://doi.org/10.5194/wes-2022-82
Preprint. Discussion started: 20 September 2022

Acknowledgements. The research presented in this paper has been funded by the Independent Research Fund Denmark (DFF) through the research project *Integrated Design of Offshore Wind Power Plants* with project nr. 1127-00188B

https://doi.org/10.5194/wes-2022-82
Preprint. Discussion started: 20 September 2022

eawe european academy of wind energy
Open Access WIND ENERGY SCIENCE DISCUSSIONS

References

Archer, R., Nates, G., Donovan, S., and Waterer, H.: Wind turbine interference in a wind farm layout optimization mixed integer linear programming model, Wind Engineering, 35, 165–175, 2011.

Baker, N., Stanley, A., Thomas, J., Ning, A., and Dykes, K.: Best practices for wake model and optimization algorithm selection in wind farm layout optimization, in: AIAA Scitech 2019 Forum, p. 0540, https://doi.org/https://doi.org/10.2514/6.2019-0540, 2019.

Bastankhah, M. and Porté-Agel, F.: Experimental and theoretical study of wind turbine wakes in yawed conditions, Journal of Fluid Mechanics, 806, 506, https://doi.org/https://doi.org/10.1017/jfm.2016.595, 2016.

Deb, K.: Optimization for Engineering Design: Algorithms and Examples, 2nd ed, PHI, 2013.

Dykes, K., Rethore, P.-E., Zahle, F., and Merz, K.: IEA Wind Task 37 Final Proposal. Wind Energy Systems Engineering: Integrated RD&D, Tech. rep., International Energy Agency, 2015.

Fagerfjäll, P.: Optimizing wind farm layout-more bang for the buck using mixed integer linear programming (MSc. Thesis), Tech. rep., Chalmers University of Technology. Department of Mathematical Sciences, 2010.

Fischetti, M. and Lodi, A.: Local branching, Mathematical Programming, 98, 23–47, 2003.

Fischetti, M., Fischetti, M., and Monaci, M.: Optimal turbine allocation for offshore and onshore wind farms, in: Optimization in the real world, pp. 55–78, Springer, 2016.

Grady, S., Hussaini, M., and Abdullah, M.: Placement of wind turbines using genetic algorithms, Renewable Energy, 30, 259–270, https://doi.org/https://doi.org/10.1016/j.renene.2004.05.007, 2005.

GWEC: Global Wind Report 2019, Tech. rep., GWEC, https://gwec.net/global-wind-report-2019/, 2020a.

GWEC: Global Offshore Wind Report 2020, Tech. rep., GWEC, https://gwec.net/wp-content/uploads/2020/12/GWEC-Global-Offshore-Wind-Report-2020.pdf, 2020b.

Herbert-Acero, J., Probst, O., Réthoré, P.-E., Larsen, G., and Castillo-Villar, K.: A Review of Methodological Approaches for the Design and Optimization of Wind Farms, Energies, 7, 6930–7016, https://doi.org/10.3390/en7116930, 2014.

IBM: IBM ILOG CPLEX Optimization Studio CPLEX User Manual, Tech. rep., IBM, https://www.ibm.com/docs/en/icos/20.1.0, 2022.

IEA Wind Task 37, I. W.: Wake Model Description for Optimization Only Case Study, Tech. rep., International Energy Agency, https://github.com/byuflowlab/iea37-wflo-casestudies/blob/master/cs1-2/iea37-wakemodel.pdf, 2019.

Investopedia: Discounted Cash Flow (DCF), https://www.investopedia.com/terms/, 2022.

Katic, I., Højstrup, J., and Jensen, N.: A simple model for cluster efficiency, in: European Wind Energy Association conference and exhibition, vol. 1, pp. 407–410, 1986.

Kuo, J., Romero, D., Beck, J., and Amon, C.: Wind farm layout optimization on complex terrains–Integrating a CFD wake model with mixed-integer programming, Applied Energy, 178, 404–414, https://doi.org/https://doi.org/10.1016/j.apenergy.2016.06.085, 2016.

Mishnaevsky Jr, L. and Thomsen, K.: Costs of repair of wind turbine blades: Influence of technology aspects, Wind Energy, 23, 2247–2255, 2020.

Mittal, P. and Mitra, K.: Decomposition based multi-objective optimization to simultaneously determine the number and the optimum locations of wind turbines in a wind farm, IFAC-PapersOnLine, 50, 159–164, 2017.

Mosetti, G., Poloni, C., and Diviacco, D.: Optimization of wind turbine positioning in large wind farms by means of a genetic algorithm, Journal of Wind Engineering and Industrial Aerodynamics, 51, 105–116, https://doi.org/https://doi.org/10.1016/0167-6105(94)90080-9, 1994.

https://doi.org/10.5194/wes-2022-82
Preprint. Discussion started: 20 September 2022

Niayifar, A. and Porté-Agel, F.: A new analytical model for wind farm power prediction, in: Journal of Physics: Conference Series, vol. 625, p. 012039, IOP Publishing, https://doi.org/10.1088/1742-6596/625/1/012039, 2015.

Nord Pool: Price Development, https://www.nordpoolgroup.com/en/, 2022.

Pearson, K.: VII. Note on regression and inheritance in the case of two parents, in: Proceedings of the Royal Society of London, vol. 58, pp. 240–242, The Royal Society London, https://doi.org/10.1098/rspl.1895.0041, 1895.

Pérez, B., Mínguez, R., and Guanche, R.: Offshore wind farm layout optimization using mathematical programming techniques, Renewable energy, 53, 389–399, 2013.

Porté-Agel, F., Bastankhah, M., and Shamsoddin, S.: Wind-turbine and wind-farm flows: a review, Boundary-Layer Meteorology, 174, 1–59, 2020.

Quan, N. and Kim, H.: Greedy robust wind farm layout optimization with feasibility guarantee, Engineering Optimization, 51, 1152–1167, 2019.

Réthoré, P.-E., Fuglsang, P., Larsen, G., Buhl, T., Larsen, T., and Madsen, H.: TOPFARM: Multi-fidelity optimization of wind farms, Wind Energy, 17, 1797–1816, 2014.

Shaw, P.: Using constraint programming and local search methods to solve vehicle routing problems, in: International conference on principles and practice of constraint programming, pp. 417–431, Springer, 1998.

Stanley, A. and Ning, A.: Massive simplification of the wind farm layout optimization problem, Wind Energy Science, 4, 663–676, https://doi.org/https://doi.org/10.5194/wes-4-663-2019, 2019.

Thomas, J. and Ning, A.: A method for reducing multi-modality in the wind farm layout optimization problem, in: Journal of Physics: Conference Series, vol. 1037, p. 042012, https://doi.org/10.1088/1742-6596/1037/4/042012, 2018.

Thomas, J., Bay, C., Stanley, A., and Ning, A.: Gradient-Based Wind Farm Layout Optimization Results Compared with Large-Eddy Simulations, Wind Energy Science Discussions, pp. 1–28, 2022a.

Thomas, J., McOmber, S., and Ning, A.: Wake expansion continuation: Multi-modality reduction in the wind farm layout optimization problem, Wind Energy, 25, 678–699, 2022b.

Turner, S., Romero, D., Zhang, P., Amon, C., and Chan, T.: A new mathematical programming approach to optimize wind farm layouts, Renewable Energy, 63, 674–680, 2014.

Wan, C., Wang, J., Yang, G., and Zhang, X.: Optimal micro-siting of wind farms by particle swarm optimization, in: International Conference in Swarm Intelligence, pp. 198–205, Springer, https://doi.org/https://doi.org/10.1007/978-3-642-13495-1_25, 2010.

Wolsey, L. A.: Integer programming, John Wiley & Sons, 2020.